Density of States of a-InGaZnO From Temperature-Dependent Field-Effect Studies

Charlene Chen, Katsumi Abe, Hideya Kumomi, and Jerzy Kanicki, *Senior Member, IEEE*

Abstract—Temperature-dependent field-effect measurements were performed on radio-frequency sputtered amorphous In–Ga–Zn–O thin film transistors (TFTs). We studied the effect of temperature on the TFT electrical properties. We observed that the field-effect mobility (μ) increases and the threshold voltage (V_T) shifts negatively with temperature, while the current on–off ratio and subthreshold slope (S) remain almost unchanged. We also observed that the TFT drain current (I_D) is thermally activated, and the relation between the prefactor (I_{D0}) and activation energy (E_a) obeys the Meyer–Neldel rule. The density of localized gap states (DOS) was then calculated by using a self-consistent method based on the experimentally obtained E_a. The result shows good agreement with the DOS distribution calculated from SPICE simulations.

Index Terms—Activation energy, amorphous In–Ga–Zn–O (a-InGaZnO), density of localized gap states (DOS), Meyer–Neldel (MN) rule, thin film transistor (TFT).

I. INTRODUCTION

OVER the past few years, amorphous In–Ga–Zn–O thin film transistor (a-IGZO TFT) has emerged as an important candidate that could be used for future flat panel displays (FPDs) [1], [2]. Aside from visible light transparency and the ability to be deposited uniformly over large area at low temperatures, a-IGZO TFTs also demonstrate favorable electrical properties, including decent field-effect mobility, high current on–off ratio, and sharp subthreshold swing [3]. All these device parameters are highly dependent on the density of localized gap states (DOS) of a-IGZO. The knowledge of these states is essential for fundamental understanding and improving the material's electrical properties. So far, such DOS has not been disclosed for a-IGZO. In this paper, for the first time [4], we report on DOS for radio-frequency (RF) sputtered a-IGZO as determined from the temperature-dependent study of the a-IGZO TFT electrical properties. Similar approach has been used to determine the DOS of amorphous silicon [5], [6] and has been proven that this method can provide meaningful information of the DOS with high reliability.

C. Chen and J. Kanicki are with the Department of Electrical Engineering and Computer Science, University of Michigan, Ann Arbor, MI 48109 USA (e-mail: Kanicki@eecs.umich.edu).

K. Abe and H. Kumomi are with the Canon Research Center, Canon Inc., Tokyo 146-8501, Japan (e-mail: Kumomi.hideya@canon.co.jp).
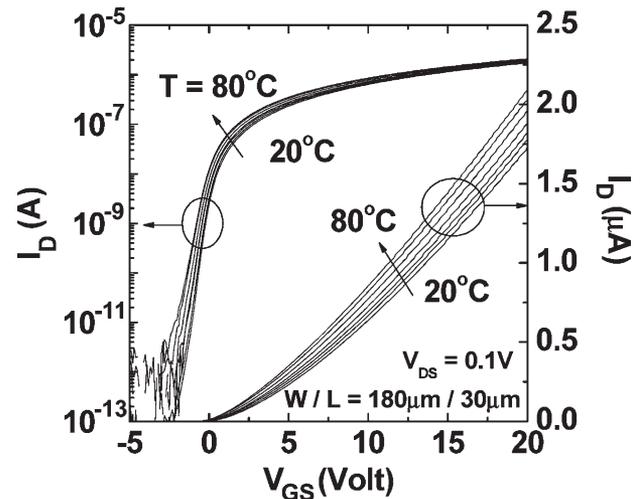
Fig. 1. a-IGZO TFT transfer characteristics (I_D–V_{GS}) measured at various temperatures, ranging from 20 °C to 80 °C.

II. TEMPERATURE-DEPENDENT FIELD-EFFECT MEASUREMENTS OF a-InGaZnO TFTs

Temperature-dependent field-effect measurements were performed on inverted–staggered RF sputtered a-IGZO TFTs. The TFTs were fabricated on glass substrates. The gate electrode Ti (5 nm)/Au (40 nm)/Ti (5 nm) was deposited by electron beam and patterned by liftoff. The gate insulator SiO_2 (200 nm) and a-InGaZnO thin film were both deposited by RF sputtering and patterned by wet etch. After annealing in air at 300 °C for 20 min, the source/drain electrodes Ti (5 nm)/Au (100 nm)/ Ti (5 nm) were deposited by electron beam and patterned by liftoff. A SiO_2 film as the back channel protection layer (100 nm) was deposited by RF sputtering and patterned by wet etch. Finally, the TFTs were annealed in air at 200 °C for 1 h [7], [8]. Measurements were done in dark, using a Hewlett-Packard 4156 A semiconductor parameter analyzer. The device temperature was regulated by a heated chuck and a Signatone temperature controller with a precision of 0.1 K. Before each measurement, the TFTs were placed on the heated chuck which is set at the desired measurement temperature for 30 min to allow for thermal equilibrium.

III. EXPERIMENTAL RESULTS

We measured the drain current (I_D) versus the gate-to-source voltage (V_{GS}) at different temperatures, ranging from 20 °C to 80 °C, as shown in Fig. 1 [drain-to-source voltage (V_{DS}) = 0.1 V]. The TFT parameters as a function of temperature are shown in Fig. 2. The field-effect mobility (μ) and threshold
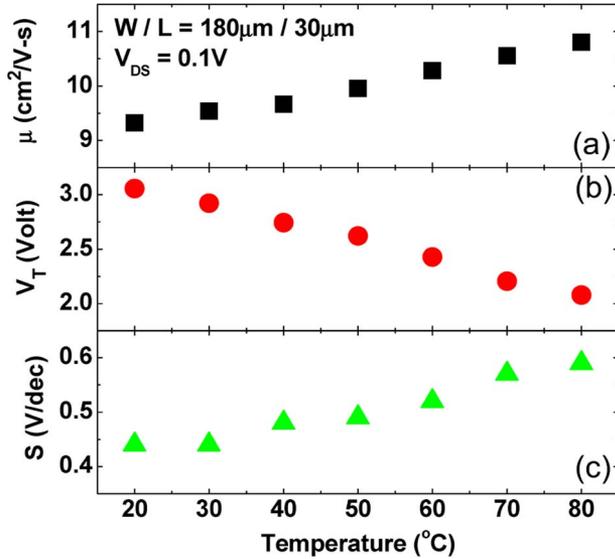
Fig. 2. Temperature dependence of the (a) field-effect mobility, (b) threshold voltage, and (c) subthreshold slope of a-InGaZnO TFTs.

Fig. 3. Temperature dependence of the drain current in (a) the subthreshold regime ($V_{GS} < 1$ V) and (b) the above threshold regime ($V_{GS} > 1$ V). Scatter dots represent the measured data; lines are used to extract E_a.

voltage (V_T) were extracted by using the standard MOSFET equation

$$I_D = \frac{W}{L} \cdot C_{ox} \cdot \mu \cdot (V_{GS} - V_T) \cdot V_{DS} \qquad (1)$$

where W and L are the channel width and length, respectively, and C_{ox} is the gate insulator capacitance per unit area. To accommodate for the nonlinearity of the I_D–V_{GS} curve, a fitting range between 10% and 90% of the maximum measured I_D is chosen [9]. From Fig. 2(a), we can see that, as the temperature rises from 20 °C to 80 °C, the field-effect mobility (μ) is weakly thermally activated and increases from 9 to 11 cm^2/V · s with a very low activation energy (E_{a_μ}) of 26 meV. Fig. 2(b) shows that the threshold voltage (V_T) linearly decreases with temperature (from 3 to 2 V) with a temperature coefficient (K_{VT}) of -17 mV/°C. The temperature dependences of μ and V_T are similar to what we commonly observed from hydrogenated amorphous silicon (a-Si:H) TFTs [10], [11], which can be explained by the multiple trapping model described by LeComber and Spear [12]: At higher temperatures, more electrons can escape from the localized states and contribute to the free carriers, which causes a higher mobility and smaller threshold voltage. The field-effect mobility and threshold voltage of a-InGaZnO TFTs are less sensitive to temperature compared to those of a-Si:H TFTs ($E_{a\_\mu} \sim 60$ meV; $K_{VT} \sim -36$ mV/°C) [10].

The subthreshold slope (S) is extracted at the steepest point of the log (I_D)–V_{GS} plot by using the following:

$$S = \left(\frac{d \log(I_D)}{d V_{GS}} \right)^{-1}. \qquad (2)$$

From Fig. 2(c), we can see that the subthreshold slope (S) slightly increases with temperature from 0.4 to 0.6 V/dec. We can also observe from Fig. 1 that the off current (I_{OFF}) almost remained the same ($10^{-12} \sim 10^{-13}$ A) within the investigated temperature range. This stable operation, even at elevated temperature, makes a-InGaZnO TFTs favorable for future FPD
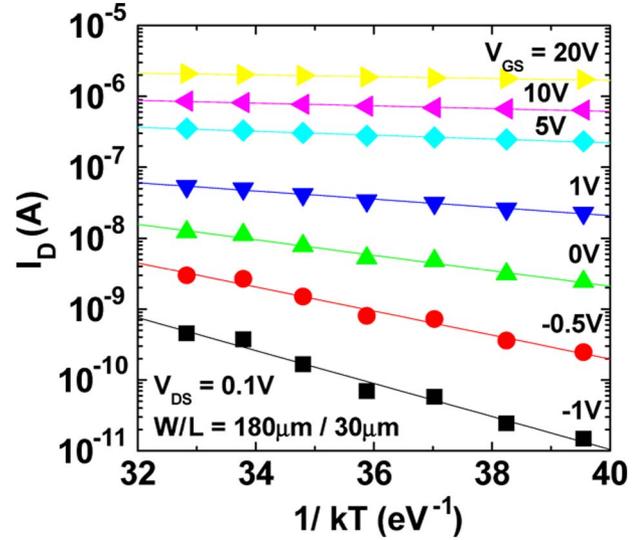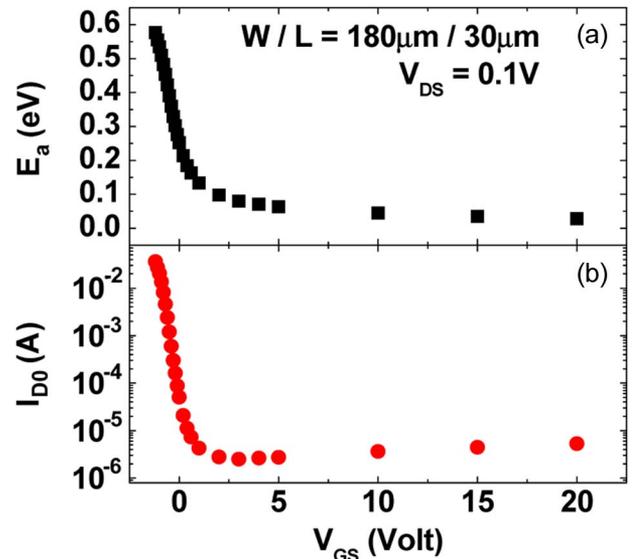

Fig. 4. (a) Activation energy (E_a) and (b) prefactor (I_{D0}) as a function of V_{GS}.

applications, which is very different from a-Si:H TFTs, where the S and I_{OFF} are very sensitive to temperature [13].

We observed that the drain current (I_D) is thermally activated and can be described by

$$I_D = I_{D0} \cdot \exp(-E_a/kT) \qquad (3)$$

where I_{D0} is the prefactor, E_a is the activation energy, k is the Boltzmann constant, and T is the temperature. I_{D0} and E_a can be easily extracted by plotting log (I_D) versus $1/kT$, as shown in Fig. 3. Both I_{D0} and E_a are V_{GS} dependent (shown in Fig. 4), and their relation obeys the Meyer–Neldel (MN) rule [14]

$$I_{D0} = I_{D00} \cdot \exp(A \cdot E_a) \qquad (4)$$

where A is the MN parameter. The MN rule is generally considered to be an intrinsic property of a material and is reported to be applicable whenever the Fermi level position is
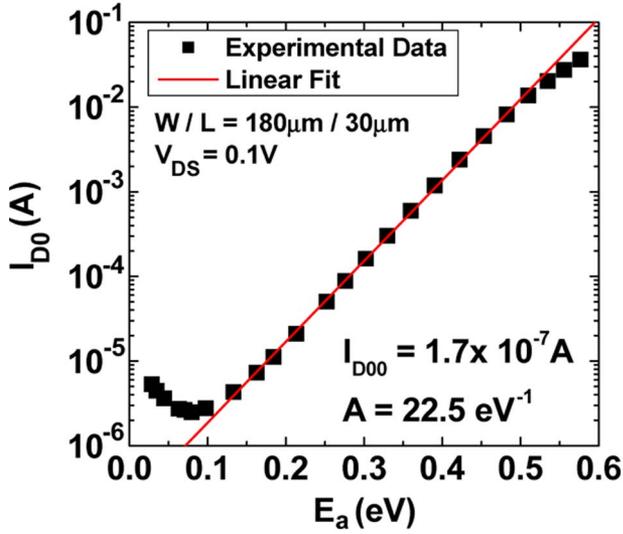
Fig. 5. Prefactor (I_{D0}) versus activation energy (E_a). Their relation can be expressed as $I_{D0} = I_{D00} \exp(A \cdot E_a)$. A is observed to be ~ 22.5 eV^{-1} in the subthreshold regime and ~ 0 eV^{-1} in the above threshold regime.

varied, regardless of whether this shift is caused by introducing extra defect states to the sample or, as in this case, by applying an electric field [6]. For our a-IGZO TFTs, as shown in Fig. 5, A is observed to be a constant (~ 22.5 eV^{-1}) over a broad range of activation energies between 0.15 and 0.5 eV, which corresponds to the subthreshold regime ($V_{GS} = -1$ to 1 V). On the other hand, in the above threshold regime ($V_{GS} > 1$ V) where the activation energy is smaller than 0.1 eV, A decreases to a value close to zero. At even lower activation energy values (< 0.05 eV), which correspond to $V_{GS} > 5$ V, A becomes negative.

IV. METHOD OF ANALYSIS

The drain current (I_D), as a function of V_{GS}, can be derived from (3) and (4)

$$I_D(V_{GS}) = I_{D00} \cdot \exp\left[(A - \beta) \cdot E_a(V_{GS})\right] \quad (5)$$

where $\beta = 1/kT$. Fig. 6 shows the energy band diagram near the semiconductor–insulator interface. The activation energy E_a is the energy difference between the Fermi level (E_F) and the edge of the conduction band (E_C), which equates to the average energy that a trapped electron needs to gain in order to escape from the localized state [15]. As we can see from Fig. 6, E_a is not only a function of V_{GS} but also a function of x (which is the distance measured from the insulator–semiconductor interface). Therefore, the activation energy extracted from $\log(I_D)$ versus $1/kT$ (shown in Fig. 4) can be seen as the "average effect" on I_D caused by $E_a(x)$ at a particular V_{GS} level. We can then rewrite (5) as

$$I_D(V_{GS}) = \frac{I_{D00}}{d_s} \cdot \int_0^{d_s} \exp\left[(A - \beta) \cdot E_a(x)\right] dx \quad (6)$$

where d_s is the thickness of the a-IGZO semiconductor layer. As shown in Fig. 6, $E_a(x)$ can also be written as $E_{aFB} - y(x)$, where E_{aFB} is the activation energy under flatband condition
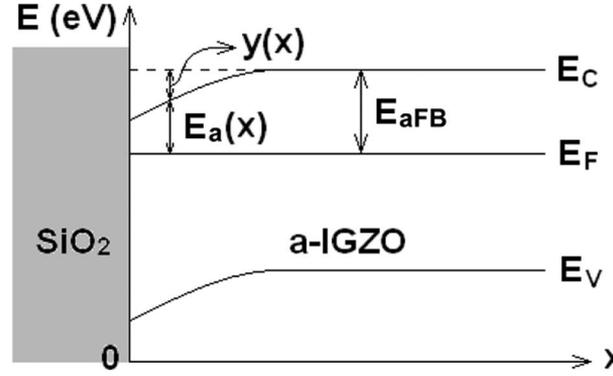

Fig. 6. Energy band diagram of an a-IGZO TFT near the semiconductor–insulator interface.

and $y(x)$ is the band bending (measured in electronvolts) caused by V_{GS} larger than the flatband voltage (V_{FB}). The drain current I_D can thus be expressed as a function of $y(x)$

$$I_D(V_{GS}) = \frac{I_{FB}}{d_s} \cdot \int_0^{d_s} \exp\left[(\beta - A) \cdot y(x)\right] dx \quad (7)$$

where

$$I_{FB} = I_{D00} \cdot \exp\left[(A - \beta) \cdot E_{aFB}\right]. \quad (8)$$

To determine the charge density (n) and the amount of band bending inside the semiconductor, Poisson equation needs to be solved for the electric field, which is related to the applied gate voltage. The Poisson equation is given by

$$\frac{d^2 y(x)}{dx^2} = \frac{e \cdot n(y)}{k_s \cdot \varepsilon_0} \quad (9)$$

where e is the absolute value of the electronic charge, k_s is the dielectric constant of the semiconductor (a-IGZO), and ε_0 is the permittivity of free space. The electric field (E) inside the semiconductor

$$E(x) = -\frac{dy(x)}{dx} \quad (10)$$

can be solved by multiplying both sides of (9) by $2dy(x)/dx$ and then integral over x. Together with the boundary conditions $y(d_s) = dy(d_s)/dx = 0$, $dy(x)/dx$ can be solved

$$\int_{d_s}^x 2 \cdot \frac{dy}{dx} \cdot \frac{d^2 y}{dx^2} dx = \int_{d_s}^x \frac{d}{dx}\left(\frac{dy}{dx}\right)^2 dx$$

$$= \int_{d_s}^x d\left(\frac{dy}{dx}\right)^2$$

$$= \left(\frac{dy(x)}{dx}\right)^2$$

$$\int_{d_s}^x \frac{2 \cdot e}{k_s \cdot \varepsilon_0} \cdot \frac{dy}{dx} \cdot n(y) dx = \frac{2 \cdot e}{k_s \cdot \varepsilon_0} \int_0^{y(x)} n(y) \, dy$$

$$\Rightarrow \frac{dy(x)}{dx} = -\left(\frac{2 \cdot e}{k_s \cdot \varepsilon_0} \int_0^{y(x)} n(y) \, dy\right)^{1/2}. \quad (11)$$

The negative sign is to make the field in the correct direction. Another boundary condition is required to solve the relation between the electric field and the applied gate bias

$$k_s \cdot E(0^+) = -k_s \cdot \frac{dy(0^+)}{dx} = k_{\text{ins}} \cdot \frac{V_{\text{GS}} - V_{\text{FB}} - y(0^+)}{d_{\text{ins}}} \tag{12}$$

where k_{ins} and d_{ins} are the dielectric constant and thickness of the gate insulator, respectively. To simplify the calculation, we assume that $y(0)$ is much smaller than $V_{\text{GS}} - V_{\text{FB}}$. Using (11) and (12), the applied gate bias can be solved as

$$V_{\text{GS}} - V_{\text{FB}} \equiv V_F = -\frac{k_s \cdot d_{\text{ins}}}{k_{\text{ins}}} \cdot \frac{dy(0^+)}{dx}$$

$$= \frac{k_s \cdot d_{\text{ins}}}{k_{\text{ins}}} \cdot \left(\frac{2 \cdot e}{k_s \cdot \varepsilon_0} \int_0^{y_s} n(y)\, dy \right)^{1/2} \tag{13}$$

where $y_s = y(0^+)$ and

$$\frac{dV_F}{dy_s} = \frac{k_s \cdot d_{\text{ins}}}{k_{\text{ins}}} \cdot \left(\frac{e}{2 \cdot k_s \cdot \varepsilon_0} \right)^{1/2} \cdot \left(\int_0^{y_s} n(y)\, dy \right)^{-1/2} \cdot n(y_s). \tag{14}$$

Using (11), we can now transform (7) into an integral over y

$$\frac{I_D - I_{\text{FB}}}{I_{\text{FB}}} = \frac{1}{d_s} \cdot \int_0^{d_s} \{ \exp\left[(\beta - A) \cdot y(x) \right] - 1 \}\, dx$$

$$= \frac{1}{d_s} \cdot \int_0^{y_s} \frac{\exp\left[(\beta - A) \cdot y(x) \right] - 1}{\left(\frac{2 \cdot e}{k_s \cdot \varepsilon_0} \int_0^{y(x)} n(y)\, dy \right)^{1/2}}\, dy. \tag{15}$$

The charge density can be solved by differentiating (15) with respect to V_F and using (14)

$$\frac{1}{I_{\text{FB}}} \cdot \frac{dI_D}{dV_F} = \frac{1}{d_s} \cdot \frac{\exp\left[(\beta - A) \cdot y_s \right] - 1}{\left(\frac{2 \cdot e}{k_s \cdot \varepsilon_0} \int_0^{y_s} n(y)\, dy \right)^{1/2}} \cdot \frac{dy_s}{dV_F}$$

$$= \frac{\exp\left[(\beta - A) \cdot y_s \right] - 1}{\left(\frac{k_s \cdot d_{\text{ins}}}{k_{\text{ins}}} \right) \cdot d_s \cdot \left(\frac{e}{k_s \cdot \varepsilon_0} \right) \cdot n(y_s)}$$

$$\Rightarrow n(y_s) = \frac{k_{\text{ins}} \cdot \varepsilon_0}{e \cdot d_{\text{ins}} \cdot d_s} \cdot \frac{I_{\text{FB}} \cdot \{ \exp\left[(\beta - A) \cdot y_s \right] - 1 \}}{dI_D / dV_F}. \tag{16}$$

Now, we can obtain $y_s(V_F)$ by plugging (16) into (14) and using (13)

$$\frac{dy_s}{dV_F} = \frac{k_{\text{ins}}}{k_s \cdot d_{\text{ins}}} \cdot \frac{V_F}{I_{\text{FB}}} \cdot \frac{dI_D}{dV_F} \cdot \frac{1}{\exp\left[(\beta - A) \cdot y_s \right] - 1}. \tag{17}$$

Integrating (17) immediately yields

$$\exp\left[(\beta - A) \cdot y_S(V_F) \right] - (\beta - A) \cdot y_S(V_F) - 1$$

$$= \frac{\beta - A}{I_{\text{FB}}} \cdot \frac{d_s}{d_{\text{ins}}} \cdot \frac{k_{\text{ins}}}{k_s} \cdot \left[V_F \cdot I_D(V_F) - \int_0^{V_F} I_D(V_F')\, dV_F' \right]. \tag{18}$$
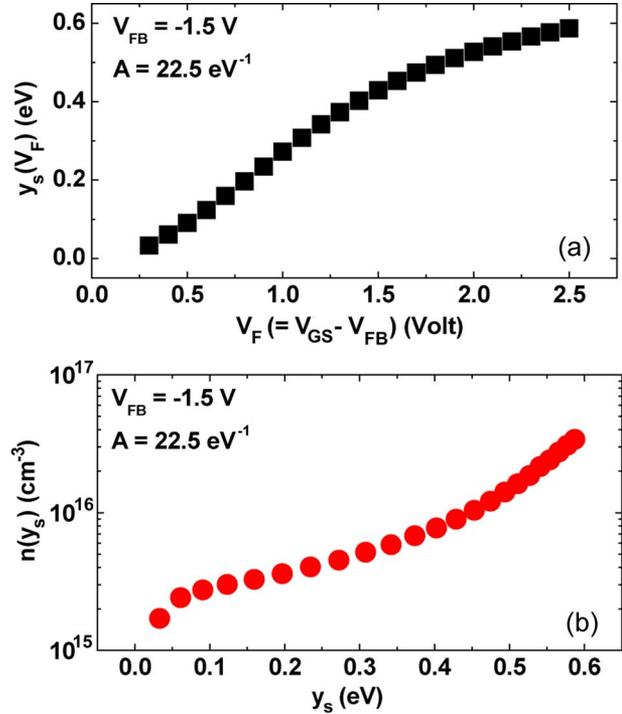

Fig. 7. Calculated (a) band bending at the semiconductor–insulator interface (y_s) as a function of $V_F (= V_{\text{GS}} - V_{\text{FB}})$ and (b) induced charge density (n) as a function of y_s.

Using (18), we can calculate the amount of band bending at the semiconductor–insulator interface $y_s(V_F)$ from experimental data $I_D(V_F)$ measured at a single temperature (in this case, 20 °C). Then, the charge density $n(y_s)$ is obtained from (16). An example of the calculated $y_s(V_F)$ and $n(y_s)$ is shown in Fig. 7. The method to determine the appropriate flatband voltage (V_{FB}) will be discussed in the next section. Finally, the DOS function $N(E)$ is calculated from

$$N(E) = \left| \frac{dn(y_s)}{dy_s} \right|_{y_s = E}. \tag{19}$$

Here, we assume that most induced charge is localized and 0-K Fermi statistics is applicable for the occupancy of the localized states. The biggest advantage of using 0-K Fermi statistics is that $N(E)$ can be easily calculated from $n(y_s)$ by differentiation. The 0-K approximation of Fermi statistics is valid when the characteristic energy of $N(E)$ is much higher than the measurement temperature (25 meV at 20 °C). This requirement can be checked by observing the calculated DOS profile. Although finer structures of the DOS can be obtained when finite temperature statistics is used, assuming a 0-K Fermi statistics is good enough for estimating the order of $N(E)$.

V. RESULTS AND DISCUSSION

A. Calculated Density of States

We calculated the DOS separately in the subthreshold and above threshold regimes of the a-IGZO TFT, as shown in Fig. 8, since the two regimes exhibit different MN relations. The calculated a-IGZO DOS from the subthreshold regime
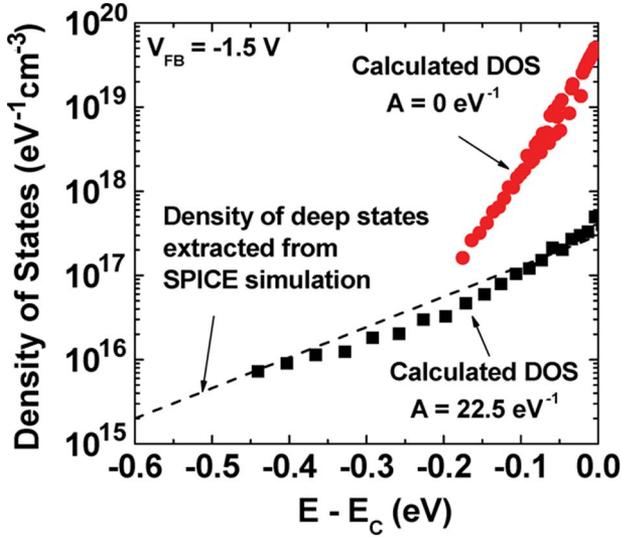
Fig. 8. Calculated DOS from both the subthreshold regime and above threshold regime as a function of $E - E_C$; $V_{\mathrm{FB}} = -1.5$ V was used.

(deep states) appears to be low ($< 10^{18}$ eV$^{-1} \cdot$ cm^{-3}) with a characteristic energy of about 120 meV. This agrees with the density of deep state profile extracted from a-IGZO TFT SPICE simulations [16], as shown in Fig. 8, where the RPI a-Si:H TFT model was used, and the DOS variation was assumed to be exponential with energy [17]. The DOS calculated from the above threshold regime (tail states) is larger and has a steeper slope with a characteristic energy of about 30 meV. The validation of the DOS calculated from the above threshold regime can be questioned for the following two reasons, which also apply to a-Si:H TFTs: 1) The free carriers can no longer be ignored in (19) and 2) the characteristic energy is very close to the measurement temperature; therefore, using 0-K Fermi statistics might lead to certain amount of error. Recognizing these limitations, we argue that the investigation of the effect of the MN parameter on the DOS profile still provides insight into the fundamental understanding of the material's electrical property.

B. Determination of the Flatband Voltage

The calculation procedure described in this paper requires the knowledge of the flatband voltage (V_{FB}). Using improper values of V_{FB} would lead to incorrect DOS. To determine the correct values of V_{FB}, we theoretically calculate the activation energy E_a as a function of V_{GS}. From (3), we can obtain

$$E_a(V_{\mathrm{GS}}) = -\frac{1}{I_D(V_{\mathrm{GS}})} \cdot \frac{dI_D(V_{\mathrm{GS}})}{d\beta} \tag{20}$$

where $dI_D(V_{\mathrm{GS}})/d\beta$ can be calculated from (15)

$$\frac{dI_D(V_{\mathrm{GS}})}{d\beta} = \frac{I_D(V_{\mathrm{GS}})}{I_{\mathrm{FB}}} \cdot \frac{dI_{\mathrm{FB}}}{d\beta} + \frac{I_{\mathrm{FB}}}{d_s} \cdot \left(\frac{k_s \cdot \varepsilon_0}{e}\right)^{1/2}$$
$$\cdot \int_0^{y_s} \frac{y \cdot \exp\left[(\beta - A) \cdot y\right]}{\sqrt{2 \cdot \int_0^y n(y') \, dy'}} \, dy. \tag{21}$$
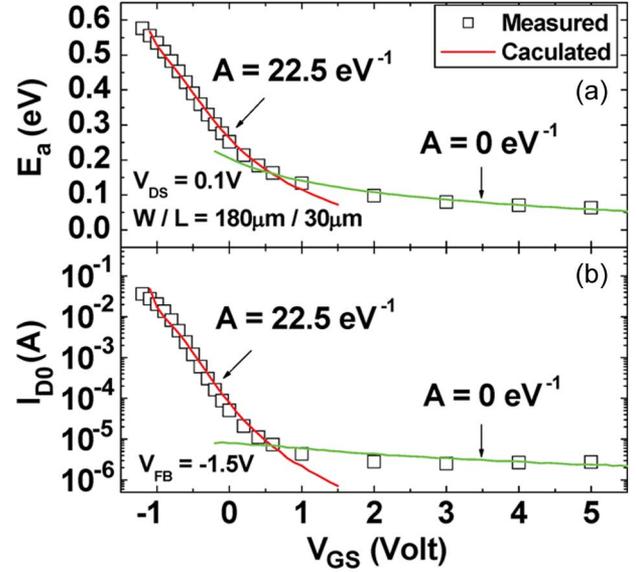

Fig. 9. Calculated and measured (a) activation energy (E_a) and (b) prefactor (I_{D0}). By using different MN parameters (A) in the subthreshold and above threshold regimes, we were able to match the calculated E_a and I_{D0} with the experimental data.

Here, we assume that the dependence of both n and y on β can be neglected in the scope of this analysis, meaning that, at any temperature (in the investigated range), most induced charge is localized and that the shift of the Fermi level with temperature is negligibly small [6]. By plugging (21) into (20), we obtain

$$E_a(V_{\mathrm{GS}}) = E_{\mathrm{aFB}} - \frac{I_{\mathrm{FB}}}{I_D(V_{\mathrm{GS}}) \cdot d_s} \cdot \left(\frac{k_s \cdot \varepsilon_o}{e}\right)^{1/2}$$
$$\cdot \int_0^{y_s} \frac{y \cdot \exp\left[(\beta - A) \cdot y\right]}{\sqrt{2 \cdot \int_0^y n(y') dy'}} \, dy \tag{22}$$

where

$$E_{\mathrm{aFB}} = -\frac{1}{I_{\mathrm{FB}}} \cdot \frac{dI_{\mathrm{FB}}}{d\beta}. \tag{23}$$

The activation energy can thus be calculated from experimental data $I_D(V_{\mathrm{GS}})$ measured at a single temperature (in this case, 20 °C), using any desired V_{FB}. A proper V_{FB} value can be obtained by matching the calculated E_a with the E_a extracted from the temperature-dependent field-effect measurements. In order to check the consistency, the prefactor I_{D0} is calculated as a function of E_a from

$$I_{D0}(V_{\mathrm{GS}}) = I_D(V_{\mathrm{GS}}) \cdot \exp\left[\beta \cdot E_a(V_{\mathrm{GS}})\right] \tag{24}$$

using the measured $I_D(V_{\mathrm{GS}})$ data and calculated $E_a(V_{\mathrm{GS}})$ values. The best fit of the theoretical calculations to the measured data is shown in Figs. 9 and 10 with $V_{\mathrm{FB}} = -1.5$ V, $E_{\mathrm{aFB}} = 0.6$ V, and $A = 22.5$ and 0 eV^{-1} in the subthreshold and above threshold regimes, respectively.

VI. CONCLUSION

We investigated the effect of temperature on RF sputtered a-IGZO TFTs. The field-effect mobility is weakly thermally
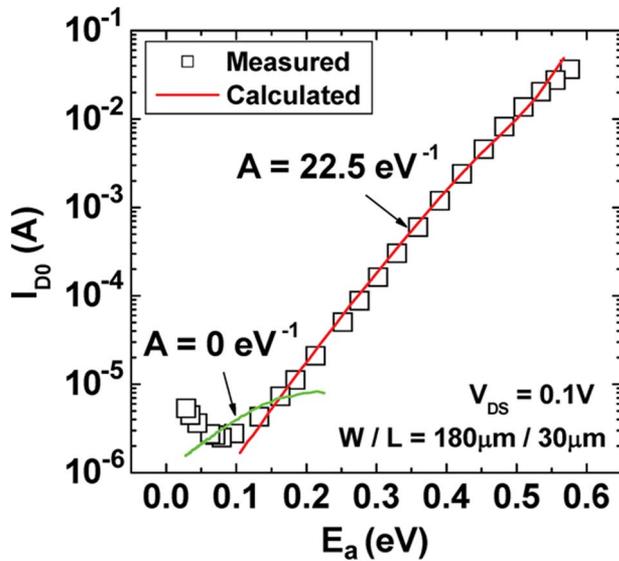
Fig. 10.   Measured and calculated prefactor (I_{D0}) as a function of activation energy (E_a).

activated (activation energy of $\sim$26 meV). The threshold voltage linearly decreases with temperature with a temperature coefficient of -17 mV/$^{\circ}$C. The current on–off ratio and subthreshold slope almost remained the same within the investigated temperature range. The density of states of RF sputtered a-IGZO was calculated by a straightforward method based on temperature-dependent field-effect measurements. The MN rule was also taken into account during the calculation. The appropriate flatband voltage and MN parameter were obtained by matching the calculated activation energy with the measured data. The calculated DOS from the subthreshold regime is low ($< 10^{18}$ eV$^{-1} \cdot$ cm^{-3}) with a characteristic energy of $\sim$120 meV and shows good agreement with the density of deep states extracted from SPICE simulations. We believe that this method provides a simple and fast interpretation of the field-effect measurements and gives us a good image of the DOS profile. More accurate results can be obtained by considering the free charge in (19) and calculating the DOS by deconvolution of the localized charge with the Fermi–Dirac distribution function.

ACKNOWLEDGMENT

REFERENCES

[1] J. Y. Kwon, K. S. Son, J. S. Jung, T. S. Kim, M. K. Ryu, K. B. Park, J. W. Kim, Y. G. Lee, C. J. Kim, S. I. Kim, Y. S. Park, S. Y. Lee, and J. M. Kim, "4 inch QVGA AMOLED display driven by GaInZnO TFT," in *Int. Display Workshop*, 2007, vol. AMD9-3, p. 1783.

[2] J. K. Jeong, J. H. Jeong, J. H. Choi, J. S. Im, S. H. Kim, H. W. Yang, K. N. Kang, K. S. Kim, T. K. Ahn, H. J. Chung, M. Kim, B. S. Gu, J. S. Park, Y. G. Mo, H. D. Kim, and H. K. Chung, "12.1-inch WXGA AMOLED display driven by indium–gallium–zinc oxide TFTs array," in *SID*, 2008, pp. 1–4. 3.1.

[3] K. Nomura, H. Ohta, A. Takagi, T. Kamiya, M. Hirano, and H. Hosono, "Room-temperature fabrication of transparent flexible thin-film transistors

using amorphous oxide semiconductors," *Nature*, vol. 432, no. 7016, pp. 488–492, Nov. 2004.

[4] C. Chen, T. C. Fung, K. Abe, H. Kumomi, and J. Kanicki, "Study of density of states of a-InGaZnO using field-effect technique," in *DRC*, 2008, pp. 151–152. III-48.

[5] M. Grünewald, P. Thomas, and D. Würtz, "A simple scheme for evaluating field effect data," *Phys. Stat. Sol. (b)*, vol. 100, no. 2, pp. K139–K143, Aug. 1980.

[6] R. Schropp, J. Snijder, and J. Verwey, "A self-consistent analysis of temperature-dependent field-effect measurements in hydrogenated amorphous silicon thin-film transistors," *J. Appl. Phys.*, vol. 60, no. 2, pp. 643–649, Jul. 1986.

[7] K. Abe, H. Kumomi, K. Nomura, T. Kamiya, M. Hirano, and H. Howono, "Amorphous In–Ga–Zn–O based TFTs and circuits," in *Int. Display Workshop*, 2007, vol. AMD9-2, pp. 1779–1782.

[8] C. Chen, K. Katsumi, H. Kumomi, and J. Kanicki, "RF sputter a-InGaZnO TFTs for flat panel displays," in *SID Vehicles Phonons*, 2008, pp. 111–115. 5-2.

[9] T. C. Fung, K. Nomura, and J. Kanicki, "PLD amorphous In–Ga–Zn–O TFTs for future optoelectronics," in *SID Vehicles Photons*, 2008, pp. 117–123. 5-3.

[10] B. Iniguez, L. Wang, A. Fjeldly, M. S. Shur, and H. Slade, "Thermal, self-heating and kink effects in a-Si:H thin film transistors," in *IEDM Tech. Dig.*, 1998, pp. 879–882.

[11] A. Kuo, T. K. Won, and J. Kanicki, "Advanced amorphous silicon thin-film transistors for AM-OLEDs: Electrical performance and stability," *IEEE Trans. Electron Devices*, vol. 55, no. 7, pp. 1621–1629, Jul. 2007.

[12] P. G. LeComber and W. E. Spear, "Electronic transport in amorphous silicon films," *Phys. Rev. Lett.*, vol. 25, no. 8, pp. 509–511, Aug. 1970.

[13] H. C. Slade, M. S. Shur, S. C. Deane, and M. Hack, "Physics of below threshold current distribution in a-Si:H TFTs," in *Proc. Mater. Res. Soc. Symp.*, 1996, vol. 420, pp. 257–262.

[14] W. Meyer and H. Neldel, "Relation between the energy constant and the quantity constant in the conductivity–temperature formula of oxide semiconductors," *Z. Tech. Phys.*, vol. 18, no. 12, pp. 588–593, 1937.

[15] T. Tiedje, J. M. Cebulka, D. L. Morel, and B. Abeles, "Evidence for exponential band tails in amorphous silicon hydride," *Phys. Rev. Lett.*, vol. 46, no. 21, pp. 1425–1428, May 1981.

[16] C. Chen, A. Katsumi, H. Kumomi, and J. Kanicki, (unpublished results).

[17] M. S. Shur, H. C. Slade, M. D. Jacunski, A. A. Owasu, and T. Ytterdal, "SPICE models for amorphous silicon and polysilicon thin film transistors," *J. Electrochem. Soc.*, vol. 144, no. 8, pp. 2833–2839, 1997.

Charlene Chen received the B.S. degree in electrical engineering from the National Taiwan University, Taipei, Taiwan, in 2005 and the M.S. degree in electrical engineering from the University of Michigan, Ann Arbor, in 2006, where she is currently working toward the Ph.D. degree at the Department of Electrical Engineering and Computer Science, under the supervision of Prof. Kanicki.

Her current research mainly focuses on a-InGaZnO TFTs and their application to active-matrix organic light-emitting displays.

Katsumi Abe received the B.S. and M.S. degrees in nuclear engineering from Kyoto University, Kyoto, Japan, in 1993 and 1995, respectively.

He has been with the Canon Research Center, Canon Inc., Tokyo, Japan, since 2003. His research focuses on amorphous oxide semiconductor TFTs and their device physics.

Hideya Kumomi received the B.S., M.S., and Dr. Sci. degrees in physics from Waseda University, Tokyo, Japan.

He is with Canon Research Center, Canon Inc., Tokyo, for about two decades. He has been working on nonlinear phenomena in phase transition, particularly on nucleation problems, and on TFTs based upon single-crystalline or polycrystalline Si and amorphous oxide semiconductors. He currently manages a laboratory for oxide semiconductors at Canon Inc. and also serves as a Committee Member of technical conferences and an Editor of scientific journals.

Jerzy Kanicki (M'99–A'99–SM'00) received the Ph.D. degree in sciences (Dr. Sci.) from the Free University of Brussels (ULB), Brussels, Belgium, in 1982. His dissertation research work involved the optical, electrical, and photovoltaic properties of undoped and doped trans-polyacetylene.

He subsequently joined the IBM Thomas J. Watson Research Center, Yorktown Heights, NY, as a Research Staff Member working on hydrogenated amorphous silicon devices for photovoltaic and flat panel display applications. In 1994, he moved from IBM Research Division to the University of Michigan, Ann Arbor, as a Professor at the Department of Electrical Engineering and Computer Science. At the University of Michigan, from 1994 to 2000, he did leading work on various flat panel displays technologies. He started working in 2000 on a variety of fundamental problems related to organic and molecular electronics. From 2002 to 2003, he spent a sabbatical year at the Center for Polymers and Organic Solids (Physics Department), University of California, Santa Barbara, conducting research in the area of conducting polymer devices. He is the author and coauthor of over 250 publications in journals and conference proceedings. He has edited two books and three conference proceedings. He is the coauthor of the book "High-Fidelity Medical Imaging Displays" (SPIE Press, 2004). He presented numerous invited talks at national and international meetings in the area of organic and inorganic semiconductor devices. More information about his research group activities can be found at www.eecs.umich.edu/omelab/.